Mechanics in Nano-Engineering 1(2) (2027) 19-45

Ministry of Science, Research and Technology
University of Bonab

Mechanics in Nano-Engineering

journal homepage: https://mneng.ubonab.ac.ir/

Mechanics in NANO-ENGINEERING

Experimental and Numerical Study on Friction Stir Back Extrusion of Recycled AA7020/Al_2O_3 Composite Rods

Elman Adhami [a], Elyas Haddadi [b,*], Hossein Jafarzadeh [c]

[a] Department of Mechanical Engineering, Faculty of Mechanical and manufacturing Engineering, University of Tabriz, Tabriz, Iran
[b] Department of Mechanical Engineering, Technical and Vocational University (TVU), Tehran, Iran
[c] Department of Mechanical Engineering, Tabriz Branch, Islamic Azad University, Tabriz, Iran

ARTICLE INFO

Article history:
Received 8 11 2026
Received in revised form 11 6 2026
Accepted 11 9 2026

Keywords:
AA7020
Friction stir back extrusion (FSBE)
Severe plastic deformation (SPD)
Finite element method (FEM)
Aluminum oxide (Al_2O_3)
Composite

ABSTRACT

In this research, the production of composite rods from recycled AA7020 alloy chips together with Al_2O_3 reinforcing particles (average particle size of 1 µm) was investigated experimentally and numerically via the friction stir back extrusion (FSBE) method. The die and punch were made of H13 steel, and heat treatment and nitriding were applied to increase wear resistance. The FSBE process was optimized at a rotational speed of 450 rpm and a feed rate of 10 mm/min. Specimens were fabricated with Al_2O_3 weight percentages of 0, 0.5, 0.75, 1, and 2%. The results showed that the addition of particles up to 1 wt.% increased the yield strength to 300 MPa and the ultimate tensile strength to 378 MPa, while increasing the content to 2 wt.% reduced these values to 250 MPa and 300 MPa, respectively. The hardness of the specimens increased from 92 HB (for the specimen without particles) to 105 HB (for the 2 wt.% specimen). Finite element simulation using DEFORM software showed good agreement with experimental results (temperature of 390–400°C). This method offers a low-energy and sustainable approach for the direct production of composite rods from aluminum scrap.

1. Introduction

conductivity, is one of the most widely used non-ferrous metals in transportation, aerospace, and construction industries [1-3]. However, the low tensile strength of pure aluminum (40-70 MPa) has driven the development of 7000-series alloys such as AA7020. These alloys achieve considerable strength through the formation of $MgZn_2$ precipitates via age hardening and solution treatment [4-6]. Moreover, alloy 7020 exhibits better weldability than other 7000-series alloys and performs well in processes like friction stir welding [7].

* Corresponding author.
E-mail addresses: ehadadi@tvu.ac.ir

http://dx.doi.org
© 2021 Published by University of Bonab

On the other hand, growing environmental and economic concerns have made the direct recycling of aluminum chips a major challenge. Traditional recycling routes based on remelting consume high energy and lead to a loss of mechanical properties [8]. In this context, solid-state processes such as severe plastic deformation (SPD) and especially friction stir extrusion (FSE) have been introduced as novel and sustainable solutions, owing to the absence of melting, lower energy consumption, and the creation of ultrafine-grained microstructures [9-11]. Previous studies have shown that FSE can directly convert aluminum chips into products with strengths close to those of the virgin material (up to ~300 MPa) [12]. Also, direct hot extrusion of chips at 400-500 °C can yield a yield strength of about 230 MPa [12,13].

In addition to recycling, the addition of ceramic reinforcing nanoparticles such as Al_2O_3 has the potential to significantly improve the hardness, wear resistance, and tensile strength of aluminum-matrix composites (Al-MMCs) [14,15]. The strengthening mechanisms include load transfer, the Hall-Petch effect, and dislocation pinning by Al_2O_3 particles [14]. Despite recent advances in friction-based processes (e.g., FSP and FSD) for producing Al-Al_2O_3 composites, important research gaps remain in the fabrication of recycled aluminum composites via FSE: non-uniform distribution of reinforcing particles, lack of predictive models linking process parameters (rotation speed, axial force, tool geometry) to final properties, insufficient experimental data on fatigue and fracture toughness, and tool wear issues in the presence of hard Al_2O_3 particles [14,16-18]. Previous numerical studies employing meshfree and finite element approaches have demonstrated that friction conditions (sticking versus sliding) and temperature distribution significantly influence material flow and product quality during friction-based extrusion processes.

Conventional routes for producing MMCs—such as stir casting, powder metallurgy, and squeeze casting—often suffer from particle agglomeration, poor interfacial bonding, and porosity [19,20]. SPD techniques, including backward-radial extrusion and cold extrusion, can refine grains and disperse particles [21,22]. Friction stir processing (FSP), derived from friction stir welding, has emerged as a powerful SPD method for surface composite fabrication [23,24]. Friction stir back extrusion (FSBE) is a relatively novel variant that combines rotational friction heating with backward extrusion to produce fully consolidated rods from chips or solid billets [25-28]. During FSBE, a rotating punch plunges into a constrained billet; the plasticized material flows upward through an annular gap between the punch and die, forming a continuous rod [29-32]. This process has been successfully applied to aluminum alloys, and recent studies have explored FSBE for recycling metal chips, offering a solid-state, energy-efficient alternative to remelting [33,34].

However, the combined use of recycled 7020 alloy and Al_2O_3 nanoparticles in the FSBE process has not yet been comprehensively investigated. While previous studies have been largely limited to material flow without reinforcing particles, the present work systematically addresses the tool wear challenge in the presence of hard ceramic particles and, through a cross-analysis of parameters such as rotational speed and feed rate, provides an optimal processing window that ensures uniform particle distribution while preventing excessive wear and porosity. For the first time, recycled 7020 alloy chips and Al_2O_3 nanoparticles are combined in an FSBE process to produce composite rods with a homogeneous microstructure and improved mechanical properties. Furthermore, by combining experimental investigations with three-dimensional finite element simulations (FEM) using DEFORM-3D software, the present study examines the thermo-mechanical behavior of the FSBE process. The numerical model is employed to investigate the effects of process parameters, particularly punch geometry and feed rate, on temperature distribution, forming forces, and material

deformation. The simulation results are subsequently compared with experimental observations to evaluate the reliability of the numerical predictions. By integrating direct chip recycling (drastically reducing energy consumption compared to remelting) with nanoparticle reinforcement without the need for secondary processes, this research offers a sustainable, low-energy, and scalable approach for continuous industrial production of aluminum composite rods, which can serve as a foundation for the development of green manufacturing lines.

2. Materials and Methods

2.1 Material

In this study, the manufacture of composite rods using recycled aluminum alloy 7020 chips together with aluminum oxide (Al_2O_3) reinforcing particles was evaluated via the friction stir back extrusion method. Recycled alloy in the form of annealed 7020 rod was procured from the market and then converted into chips through machining operations (Figure 1). The chemical composition of the AA7020 is shown in Table 1. Aluminum oxide powder with an average particle size of 1 µm was used (Figure 2). The morphology of the aluminum oxide particles, along with the alpha phase, is also shown in Figure 2.

The recycled AA7020 chips were obtained through machining of an annealed AA7020 aluminum rod. The resulting chips exhibited an irregular, fragmented, and discontinuous morphology, consisting of small, separate pieces rather than long continuous strips (Figure 1). Before processing, the chips were washed with alcohol to remove surface contaminants and then completely dried. Subsequently, batches of 35 g were prepared for billet fabrication.

Table 1. Chemical composition of AA7020 aluminum alloy

Element	Al	Zn	Mg	Mn	Cr	Fe	Si	Cu	Zr	Zr+Ti
AA7020 (wt. %)	Bal.	4-5	1-1.4	0.05-0.5	0.1-0.35	0.4	0.35	0.2	0.08-0.2	0.8-0.25



Figure. 1. Recycled AA7020 aluminum alloy ingot and the chips produced from it

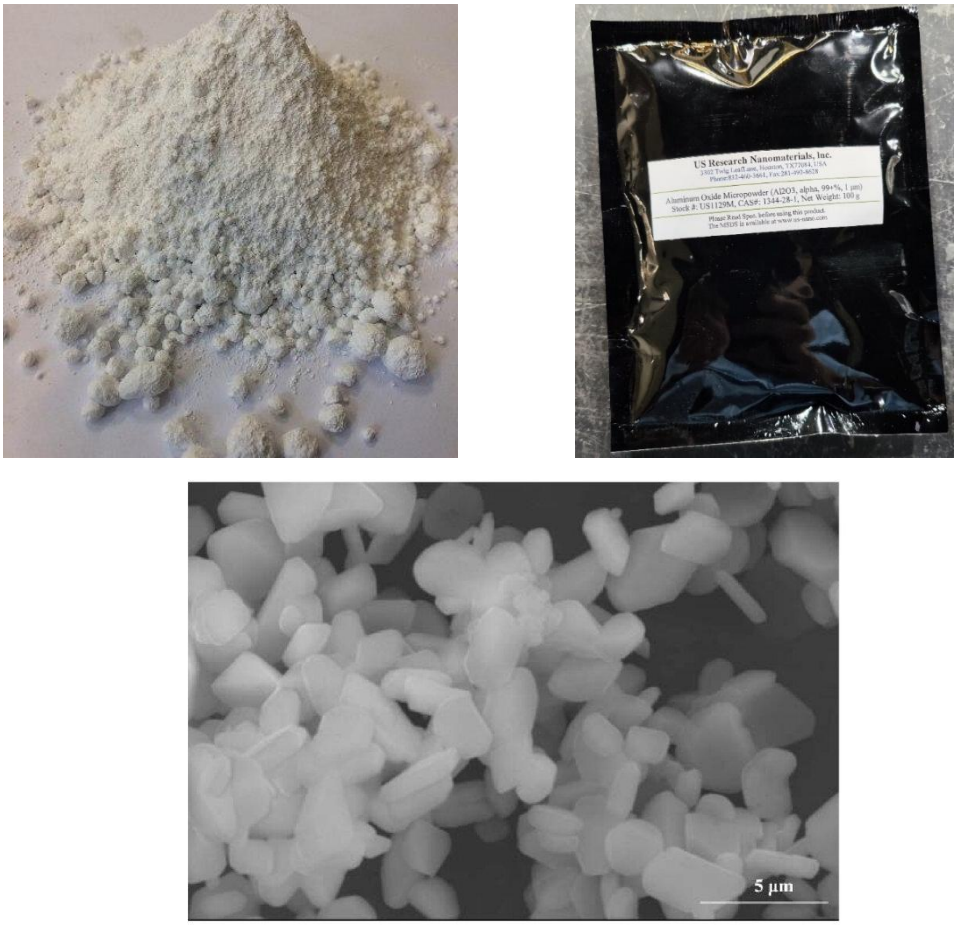


Figure. 2. Morphology of the α-Al_2O_3 particles used in this study, with an average particle size of 1 µm.

The chips obtained from the machining operation were washed with alcohol to remove impurities and contaminants from the annealed AA7020. After washing and completely drying the chips, batches weighing 35 g were prepared according to the required number of specimens. Specimens of pure AA7020 and those with different weight percentages of aluminum oxide (0.5, 0.75, 1, and 2 wt.%) were compacted using a cylindrical die with a diameter of 30 mm and a height of 50 mm via a pressing operation to produce billets (Figure 3). These billets were then used for the friction stir back extrusion process. This pressing operation was carried out using a hydraulic press with a force of 18 tons (Figure 3).



Figure. 3. Hydraulic press and die used for billet preparation, showing the pure aluminum billet and Al_2O_3-reinforced aluminum billets.

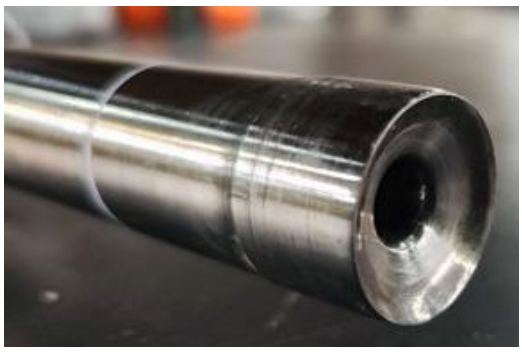
2.2 Die and Punch Design

For fabricating the die assembly, H13 steel (grade 1.2344) was selected exclusively (Figure 4). The components were designed to tolerate both compressive stresses and high temperatures. All required machining operations were performed on the parts. Given the significant thermal load acting on the matrix and the potential for component wear, a hardening heat treatment was applied to the die's critical areas. Afterwards, a nitriding process increased the surface hardness of these areas to 60 HRC. A clearance of 0.25 mm was maintained between the die and the punch. The outer shells of the die, which are subjected to lower stress levels, were also fabricated from H13 steel, whereas the inner shell and the punch were machined from the same material. Both the inner shell and the punch underwent nitriding, achieving a nitride penetration depth of 0.03 mm beneath the steel surface. The purpose of this treatment was to reduce metal adhesion on the surfaces.

The punch geometry adopted was a punch tip with a radius of 20 mm, manufactured from H13 steel (Figure5). Following the machining of the punch, a copper template conforming to the tip profile was produced to aid in achieving the required shape. Next, electrical discharge machining (EDM) was used to create the tip geometry (Figure 5b). In the absence of this precise geometry, oxidation of the aluminum chips and aluminum oxide particles in that area becomes highly likely. Consequently, the extruded wire would become fully oxidized before exiting the extrusion setup, making it unusable.



Figure. 4. Assembled die set after heat treatment and nitriding





(a) (b)



(c)

Figure. 5. (a) Punch used in the extrusion process, (b) electrical discharge machining (EDM) to produce the required geometry at the punch tip, and (c) two H13 steel punches after heat treatment and nitriding.

On the outer surface of the punch, at a distance of 20 mm from its tip, a step with a depth of 0.5 mm (diameter reduction) and a length of 50 mm along the punch axis was formed. This step resulted from localized temperature rise and thermal expansion of the punch during the process. The temperature-induced dimensional changes caused severe contact and wear between the punch and the inner wall of the die. As wear progressed, the punch gradually seized, and its movement inside the die was seriously disrupted. Under such conditions, continuation of the process became impossible, and tool replacement was required (Figures. 5a and 6)

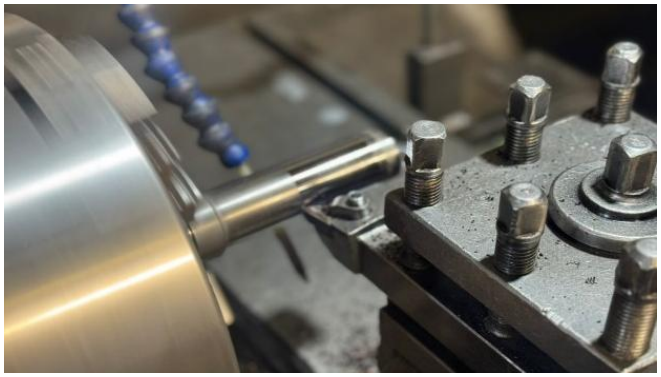


Figure. 6. Formation of a 0.5-mm step on the punch outer surface due to seizure caused by thermal expansion and wear of the die wall.

Due to certain issues that arose during the process (chips escaping from the side of the punch because of excessive clearance between the punch and the matrix, and chips not being guided toward the

hole), it was decided to manufacture a new punch with modifications. The new punch was made with a spiral on its face to better guide chips toward the hole. A CNC milling machine was used to create the spiral on the punch (Figure 7).

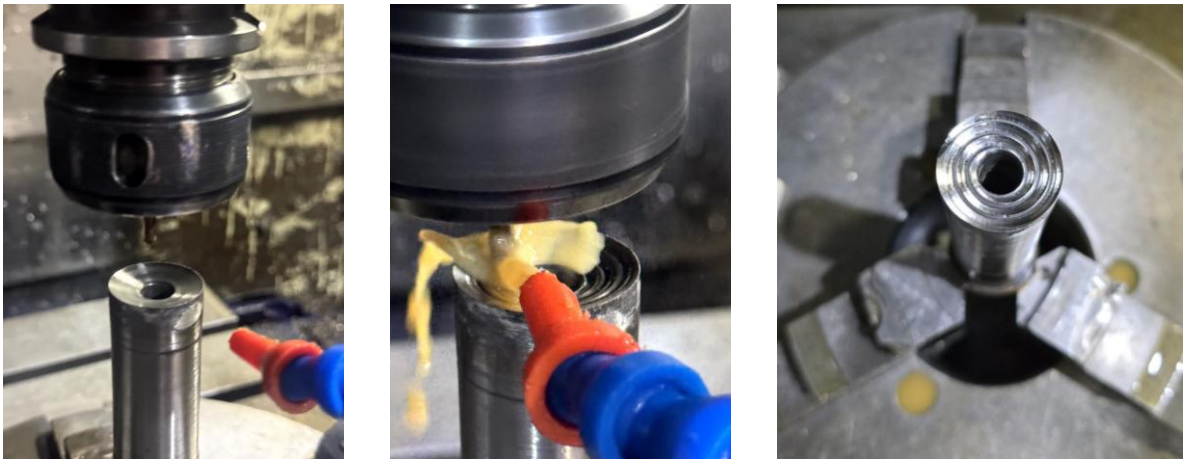


Figure. 7. Machining of the spiral groove on the second punch

2.3 FSBE Process

The prepared die and punch were mounted on milling machines—a German Deckel (Figure 8a) and a Czech FGS32 (Figure 8b)—and aligned coaxially; the Czech FGS32 proved superior due to its higher power. To verify the proper functioning of the die and punch, preliminary test runs were carried out using a plasticine specimen. After aligning the die components and ensuring their correct operation, the prepared billets of pure AA7020 and its composites were employed for the friction stir back extrusion process. Once the billets were placed inside the die, the friction stir back extrusion process was conducted using a punch rotating at 450 rpm and a feed rate of 10 mm/min. To increase the friction between the punch and the surface of the billet material, and consequently the frictional heat, at the beginning of the friction stir back extrusion process, immediately after the punch contacted the upper surface of the billet inside the die and an initial force was applied, the punch feed rate was halted. After the temperature rose to 150 °C and sufficient friction was generated, the punch advanced into the billet. Temperature was monitored using a K-type thermocouple embedded 2 mm below the punch-billet interface, recorded at 10 Hz. At this stage, with the rotation of the punch and its movement inside the die, the AA7020 reached its plastic temperature, and the friction stir back extrusion process proceeded. As the material flowed into the aperture of the punch, the extrusion of the material from the die commenced. Once the wire was formed, its temperature decreased to ambient temperature, and by reducing the feed rate and diminishing the engagement between the punch and the die, the extrusion process was completed. It should be noted that after completing the extrusion process for each specimen, the die and punch were prepared for subsequent tests through machining operations.



(a)



(b)



(c)

Figure. 8. Experimental setup and punch–die assembly on the milling machines: (a) German Deckel milling machine, (b) Czech FGS32 milling machine, and (c) execution of the forming operation.

A key challenge in the process was AA7020 sticking to the die wall and the punch wall and face. To prevent this, Die Coat liquid (typical composition of water-based die lubricant for aluminum die casting) was used [35,36]. Die Coat is a colored coating that forms a crystalline layer on the die surface, preventing adhesion (commonly used in AA7020 casting). Application method: The die and punch are heated to 200–250°C, then Die Coat is sprayed onto the desired surfaces (die wall, punch wall and face), forming a layer (Figure 9).



Figure. 9. Sequential steps involved in applying the die coating layer.

The temperature parameter was monitored throughout the entire process. An increase in temperature was observed during the process, and the maximum temperature was 390–400 degrees (Figure 10).

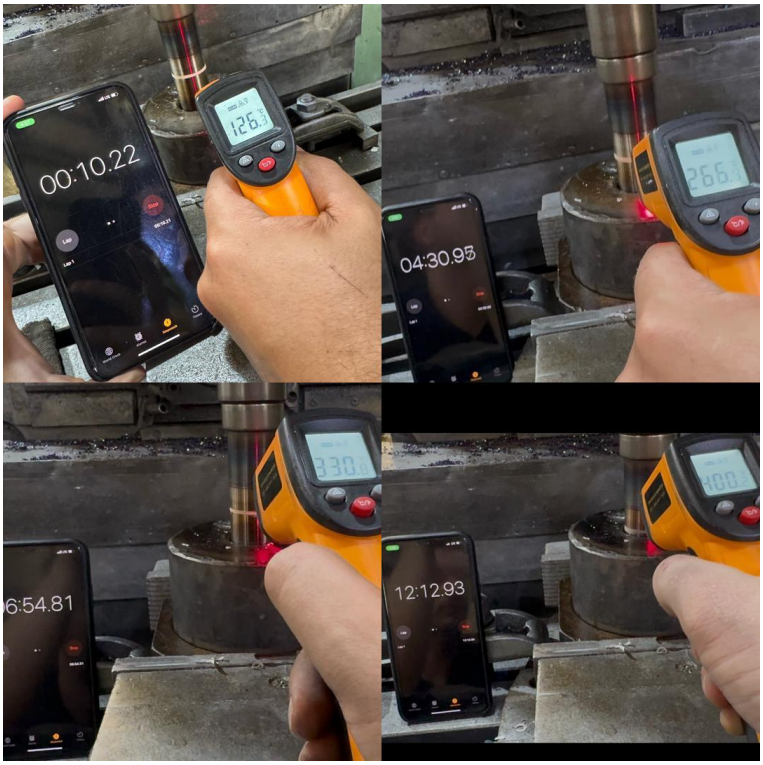


Figure. 10. Temperature measurements recorded during the experimental tests.

After producing the composite rods, the specimens were evaluated in terms of dimensions, appearance, density, microstructure, and, if necessary, mechanical properties (hardness, flexural strength, tensile strength) (Figure 11).



Figure. 11. Visual comparison of defect-free and defective specimens.

3. Finite Element Modeling

To analyze certain numerical parameters—specifically, the influence of punch tip geometry on forming forces and the temperature gradient—version 10 of the DEFORM software was used. For this purpose, all die assembly components, originally modeled in SolidWorks, were imported into DEFORM as STL files. In the simulation, the workpiece was defined as a plastic material, whereas the remaining die assembly parts were set as rigid bodies. All input values and parameters were entered in SI units within the software. Furthermore, the heat transfer mode was turned on for all die assembly components via the simulation control panel (Figure 12). Each component of the die assembly was discretized using 8,000 tetrahedral elements. To ensure mesh independence, several simulations with different element counts were conducted, and the resulting force values were compared across these meshes. Based on Figure 13, an optimal element count of 8,000 was adopted for the simulation.

The punch was driven into the specimens at a speed of 10 mm/min, consistent with the experimental setup, while the die was considered stationary throughout the simulation. The contact conditions were defined using the HOT FORGING DRY friction model available in DEFORM-3D, with a friction factor of 0.7. This friction model was applied uniformly to the relevant contact interfaces between the workpiece, punch, and die. Heat transfer was activated for the die assembly components, using a heat transfer coefficient of 11 N/(sec·mm·°C).

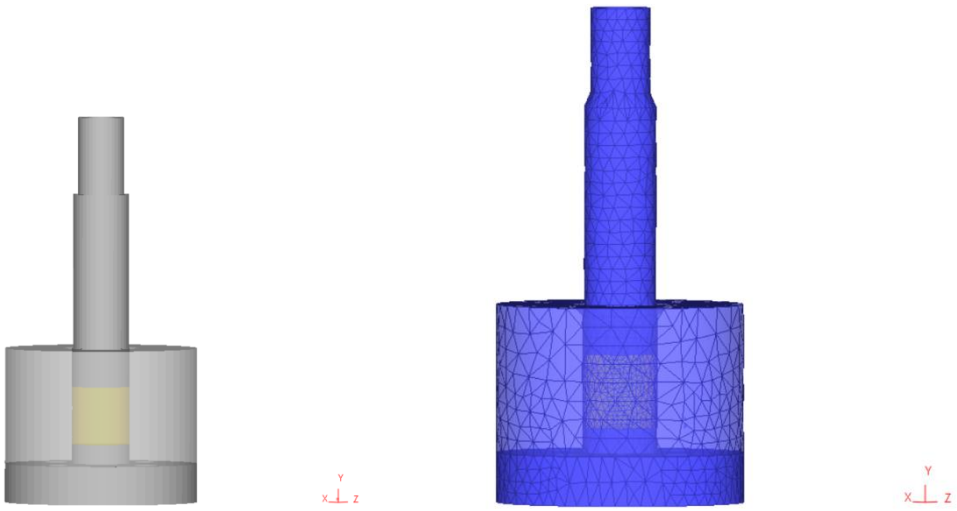


Figure. 12. Assembled die components and the corresponding meshed model in DEFORM-3D.

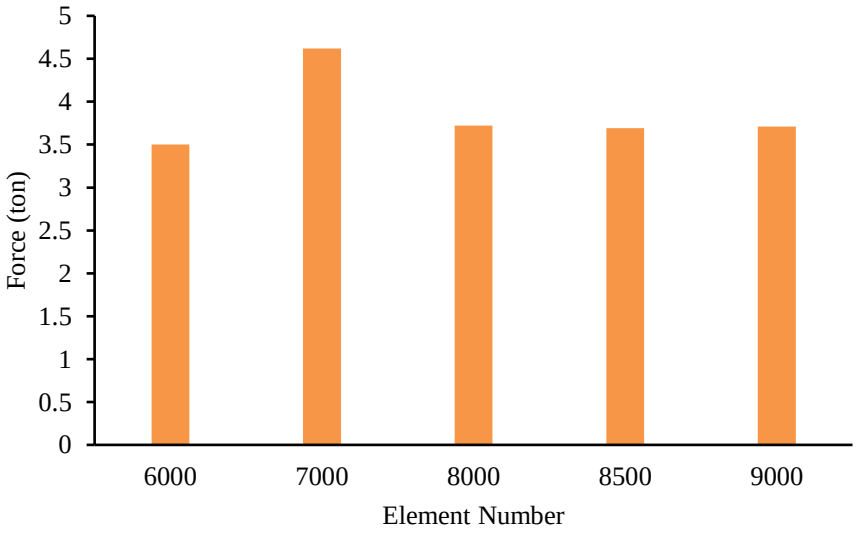


Figure. 13. Mesh independence study based on the forming force

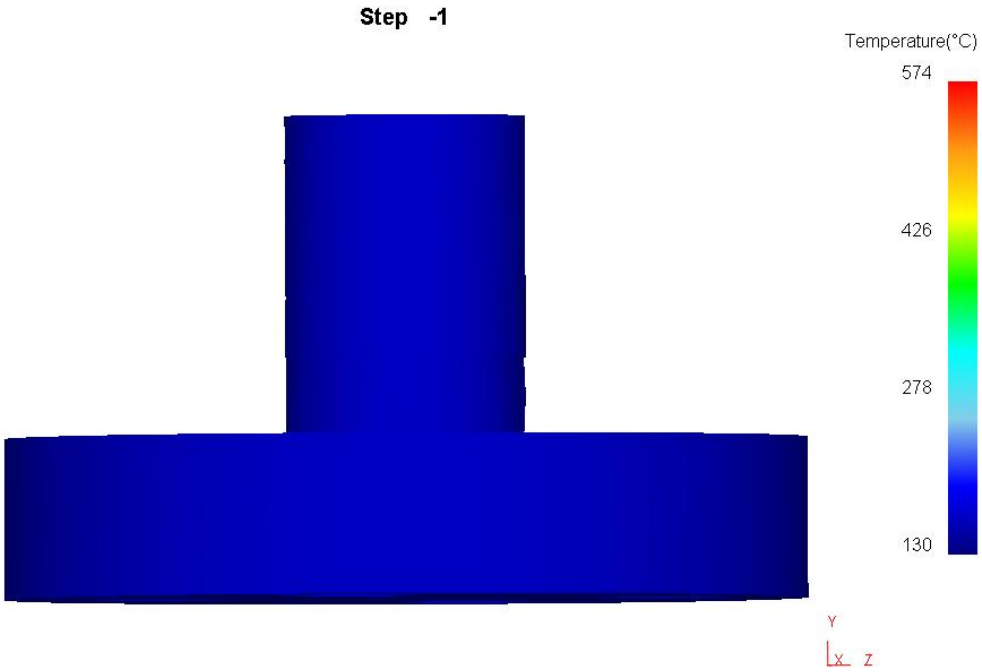
Numerical simulation of the friction stir extrusion process for AA7020 aluminum was performed in 3D-Deform software to further investigate the process parameters. Figures 14 to 19 show the distribution of temperature, load prediction, effective strain, material flow velocity, and effective stress during the simulated process.

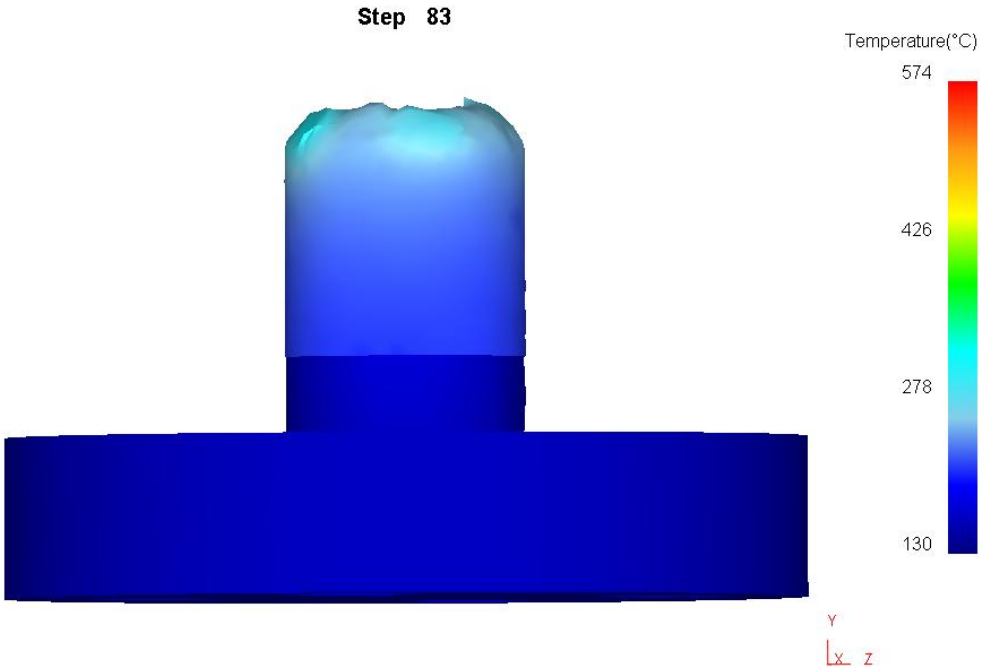
In the temperature distribution simulation, the maximum value is reached in the contact region between the punch and the starting material (approximately 380–420°C). This temperature value agrees well with the experimentally recorded temperature (about 390–400°C). The difference between the software-predicted and experimental temperature is attributed to the measurement method—in the experimental setup, due to the closed nature of the process, the temperature was measured from the outside of the punch. This temperature is sufficient to create a semi-solid state in the AA7020 alloy. Furthermore, the maximum temperature is concentrated in the central region of the punch and gradually decreases along the material flow path. This pattern confirms the correctness of the selected rotational speed (450 rpm) and feed rate (10 mm/min) in the laboratory experiment.

The effective strain is highest at the center of the part and along the extrusion path (exit channel), while the strain is lower at the edges. Regions with high strain indicate intense plastic deformation, which is favorable for grain refinement. These observations are consistent with the metallographic images of the actual specimens (grain refinement with increasing Al_2O_3 content). Non-uniform strain distribution may be a factor in the agglomeration of reinforcing particles in some specimens (e.g., the 2 wt.% specimen.

Around the punch tip, the effective stress reaches its highest value. In the middle section of the part and the exit channel, the stress value decreases. High stresses in the tool contact zone cause severe material deformation. These stresses facilitate better distribution of the reinforcing particles. However, in some cases (especially in the 2 wt.% specimen), stress concentration can lead to material sticking or surface defects.

The numerical simulation of the friction stir back extrusion process using DEFORM-3D software showed very good agreement with the experimental data obtained in the laboratory. The predicted temperature values, material flow pattern, regions of stress and effective strain concentration were fully consistent with the experimental observations. This numerical analysis demonstrated that the modified tool design, optimal rotational speed (450 rpm), and appropriate feed rate significantly contributed to optimizing the FSBE process. Finally, numerical analysis is a powerful tool for predicting material behavior and refining process design.





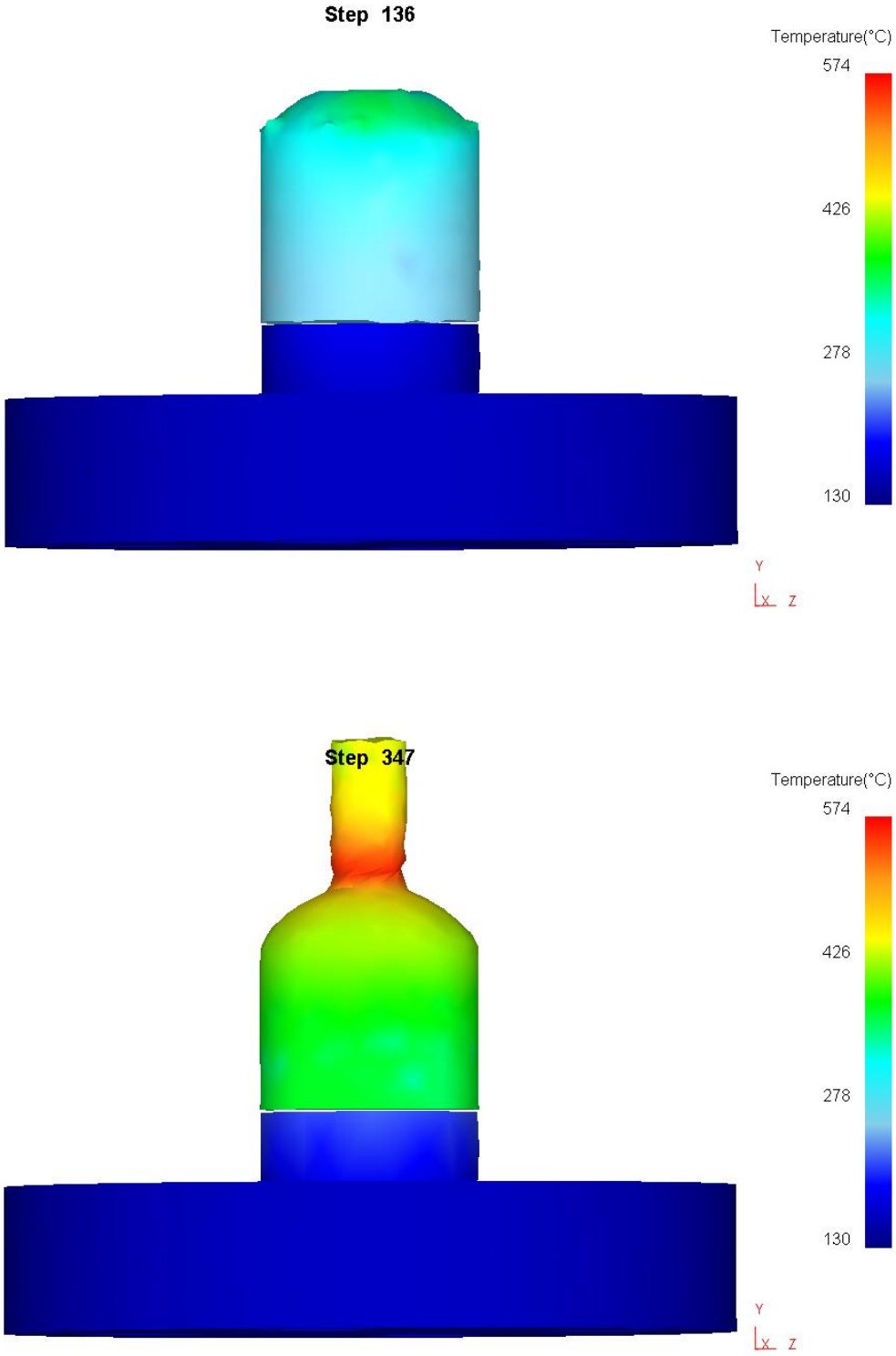


Figure. 14. Temperature distribution in the workpiece during FSBE

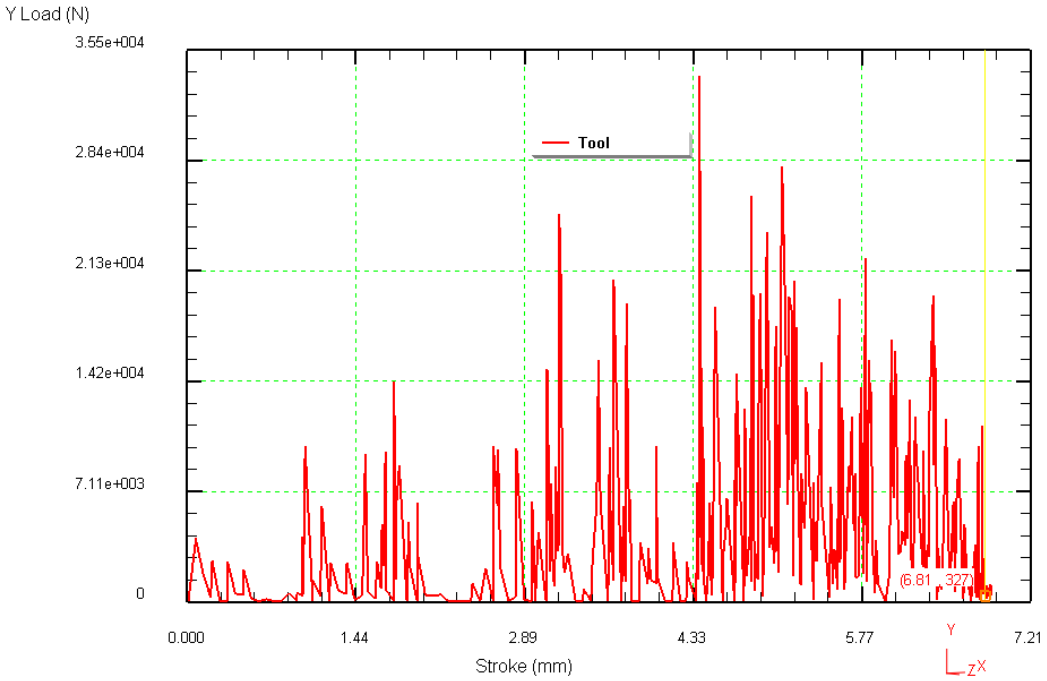


Figure. 15. Load diagram at different stages of the FSBE process

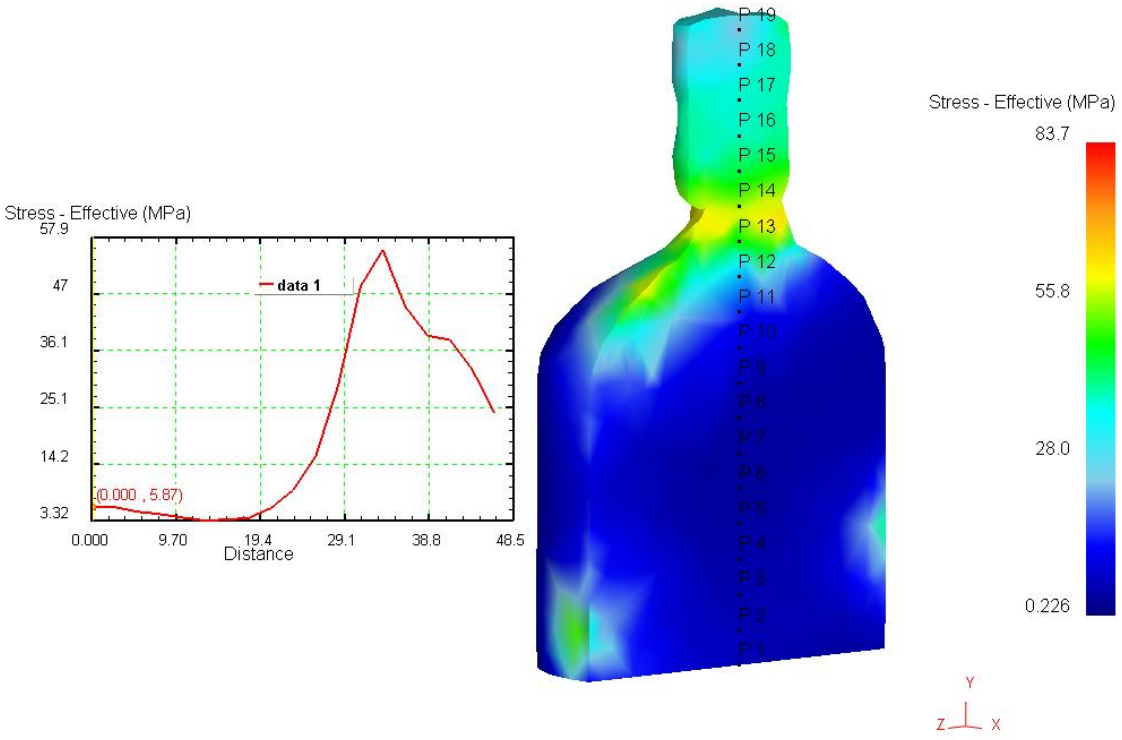


Figure. 16. Distribution of combined stresses in the vertical direction within the workpiece during FSBE

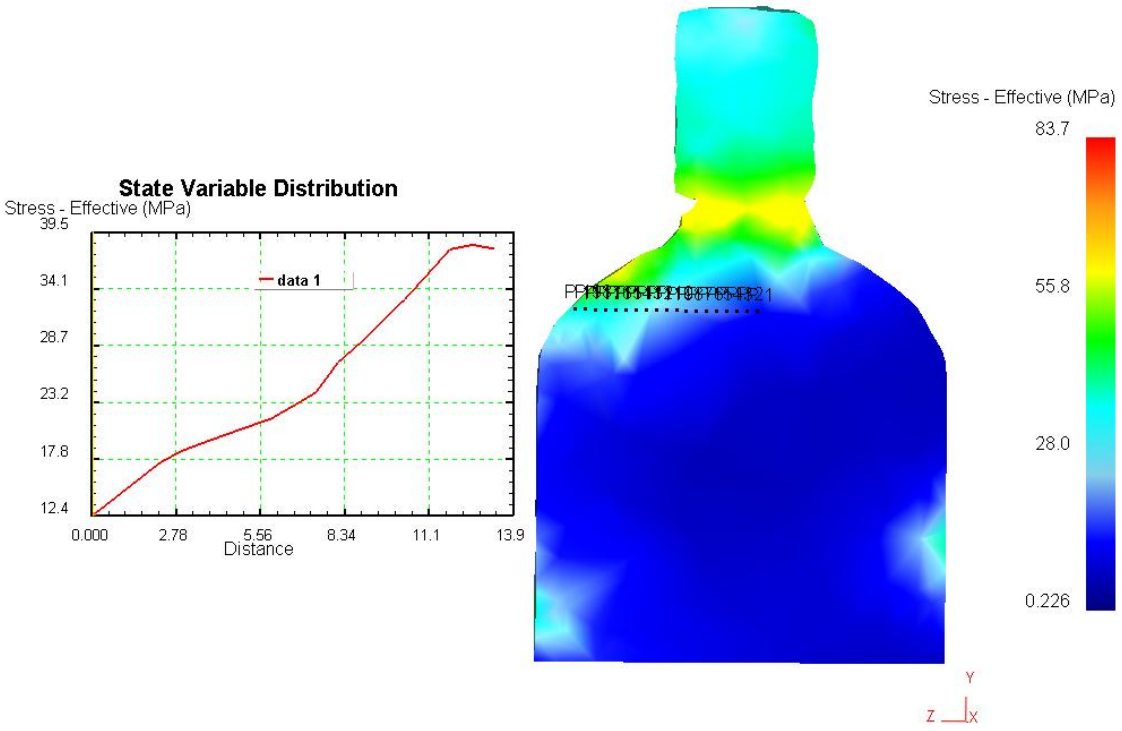


Figure. 17. Distribution of combined stresses along the horizontal axis of the workpiece

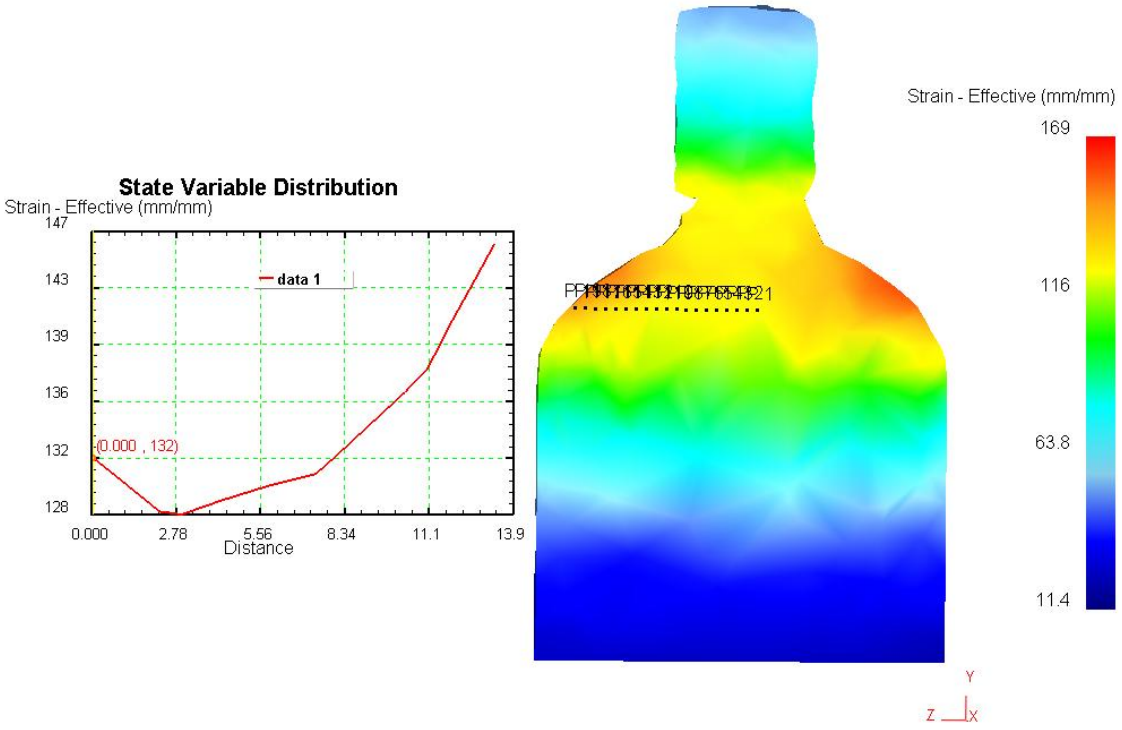


Figure. 18. Effective strain distribution along the horizontal axis of the workpiece

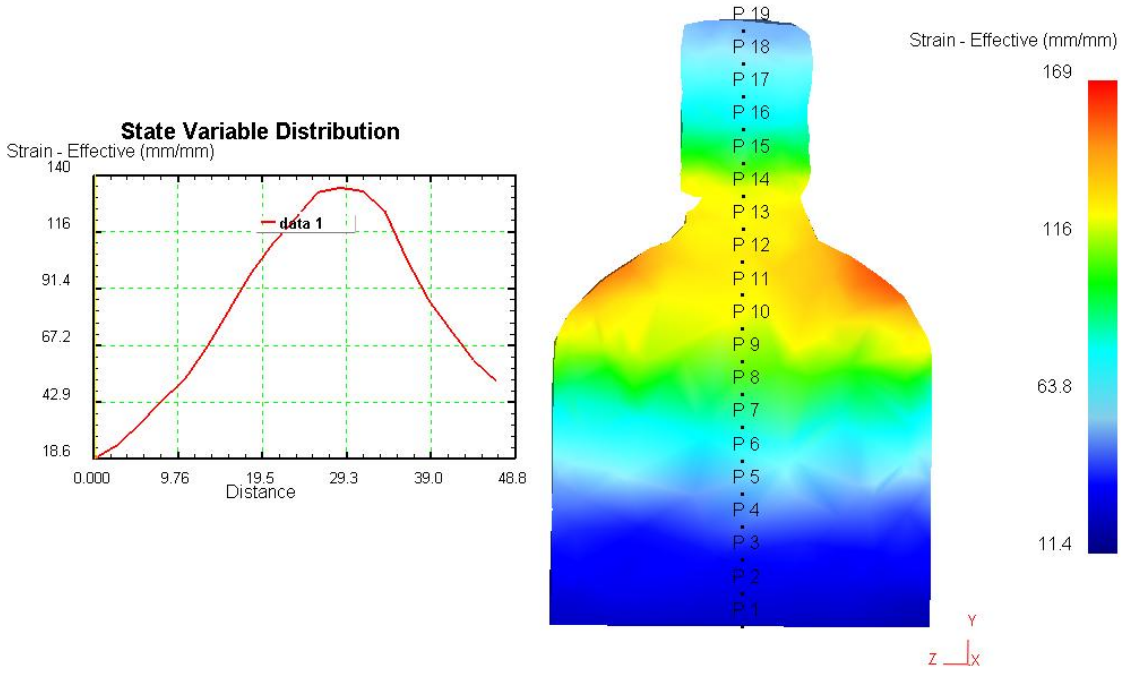


Figure. 19. Effective strain distribution along the vertical axis of the workpiece

4. Results and Discussion

4.1 Optimal Parameters of the FSBE Process

The optimal main parameters, such as tool rotational speed (300–750 rpm), axial pressure (manual and automatic feed), and feed rate, were determined through trial and error. Ultimately, a rotational speed of 450 rpm and an automatic feed rate of 10 mm/min yielded the best conditions for the friction stir back extrusion process. Table 2 presents the effect of various parameters on the process.

It should be noted that all processing conditions listed in Table 2 were experimentally investigated in the present study. The rotational speed of 450 rpm and the feed rate of 10 mm/min were selected based on the experimental observations, considering the stability of the extrusion process and the uniformity of the resulting rods. This combination provided the most favorable outcome among the investigated conditions and was therefore used for the subsequent experiments and numerical simulations.

Table 2. Process parameters investigated in this study

Rotational Speed (rpm)	Feed Rate (mm/min)	Result	Remarks
180	Manual	Unsuccessful / Chip escape	Too low friction; chips pulverized inside the die and escaped from the side of the punch
355	10	Unsuccessful / Chip compression inside the die	Insufficient temperature due to low friction; material compressed inside the die
355	16	Unsuccessful / Machine stalling	Insufficient temperature and high applied force
450	Manual	Partially successful / Non-uniform structure	Irregular extrusion due to non-uniform manual feed
450	10	Successful / Optimal	Stable extrusion, uniform structure
450	14	Partially successful	High pressure on chips; slight chip escape
560	10	Unsuccessful / Delamination	Adequate temperature rise but delamination due to high rotational speed relative to feed rate
560	14	Fair / Irregular structure	Better structure and less delamination compared to the previous case
720	10, 14 & 16	Unsuccessful / Section opening (rupture)	Very high temperature, excessive material softening, high flow rate, and opening after the extruded section (flower-like structure)

4.2 Tensile Test

Tensile test specimens were prepared according to ASTM E8/E8M standard (Fig 20). The specimens were examined with aluminum oxide weight percentages of 0%, 0.5, 0.75, 1%, and 2%. Tensile tests were also conducted on annealed AA7020 and AA7020-T6 specimens for comparison with the other specimens.

Figure 21 presents the tensile test results for various specimens. For each composition, at least 5 tensile specimens were tested, and the average values are reported. The strength values exhibited a significant increase upon the addition of Al_2O_3 reinforcing particles. The yield strength of the specimen containing 0.5 wt.% reinforcing particles was 280 MPa, which increased to 300 MPa when the particle content was raised to 1 wt.%, corresponding to an improvement of approximately 7%. However, a further increase in reinforcement content to 2 wt.% led to a reduction in yield strength to 250 MPa. A similar trend was observed for the ultimate tensile strength. At 0.5 wt.% reinforcement, the ultimate tensile strength was 355 MPa, which increased to 378 MPa at 1 wt.%, and then decreased to 300 MPa at 2 wt.%. In contrast, the elongation of the specimens showed a decreasing trend compared to the pure specimen (10%), reaching 7% for the specimen reinforced with 2 wt.% Al_2O_3 particles, indicating a 30% reduction. Nevertheless, excessively increasing the Al_2O_3 content to 2 wt.% reduces the ultimate strength of the composite. It should be noted that the decrease in strength can be attributed to factors such as material inhomogeneity, the formation of precipitates within the material, or the development of fatigue cracks and voids resulting from aluminum oxidation. The reduction in ductility (%El) of the fabricated specimens can be related to the presence and persistence of crushed oxide networks within the microstructure produced by FSBE.

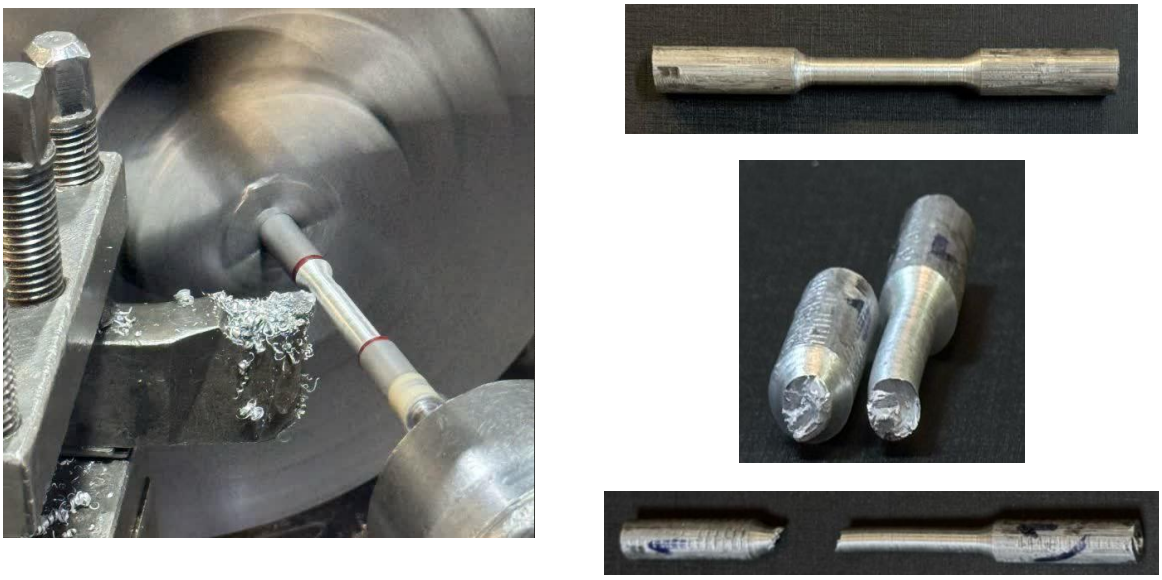


Figure. 20. Representative example of tensile specimen preparation and fracture surface examination.

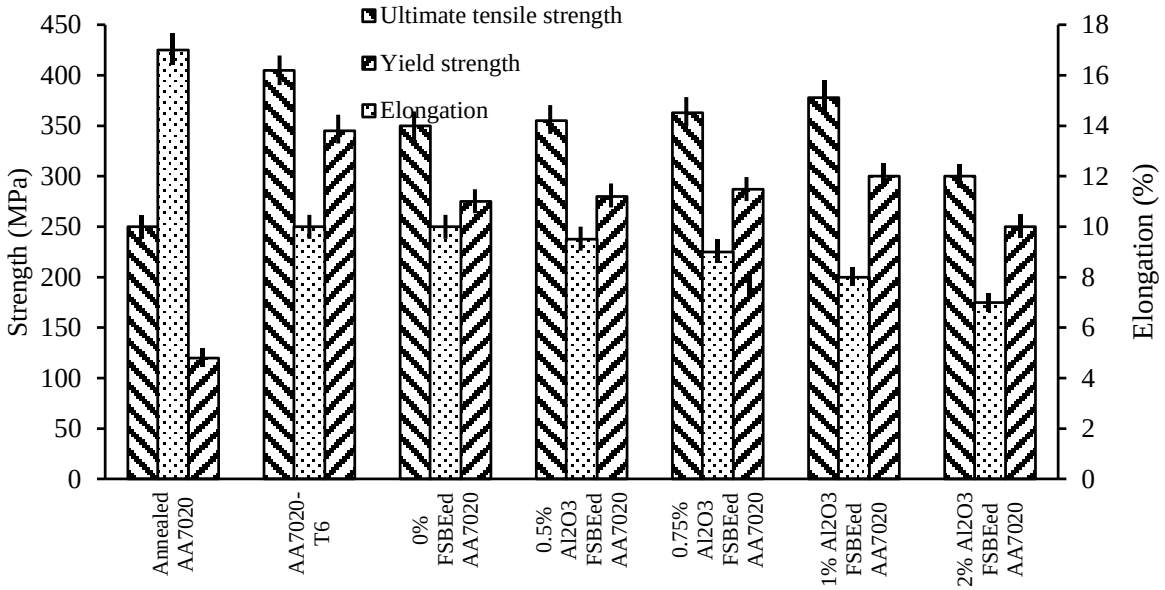


Figure. 21. Tensile test results obtained for the specimens.

4.3 Microstructural Analysis

Figure 22 presents metallographic results of the specimens produced with various weight percentages of aluminum oxide, at magnifications of 100×, 250×, and 400×. In the 0.75 wt.% specimen, the reinforcing particles are distributed in a relatively more uniform manner, although some local agglomerations are still observed. Upon reaching 1 wt.%, the microstructure becomes more homogeneous and the grains become finer, indicating the positive effect of an optimal presence of Al_2O_3 particles in effectively hindering grain growth. In the 2 wt.% Al_2O_3 specimen, the metallographic images reveal localized particle agglomeration and clustering, indicating a less uniform particle distribution compared with the specimens containing lower reinforcement contents.

Such agglomerations may act as local stress concentration sites and potentially contribute to premature failure under tensile loading. Although porosity may also influence the mechanical performance of the composite, its presence and volume fraction were not quantitatively determined in the present study. Therefore, the reduction in tensile strength observed at 2 wt.% Al_2O_3 is primarily discussed in relation to particle agglomeration and microstructural inhomogeneity, while the possible contribution of porosity requires further investigation. Overall, the metallographic images demonstrate that the friction stir extrusion process has been able to disperse Al_2O_3 particles within the AA7020 matrix; however, a more uniform particle distribution is better observed at lower percentages (0.5 to 1 wt.%). These results are consistent with the gradual increase in mechanical properties such as hardness and tensile strength, and confirm the direct influence of microstructure on improving the mechanical behavior of the specimens. The results are briefly summarized in Table 3.

Figure 23 shows the mounted specimens prepared for metallographic examination prior to etching. As can be seen, the specimens were carefully mounted to ensure a flat and representative surface for microstructural observation, which was essential for obtaining reliable metallographic images (Figure 22)

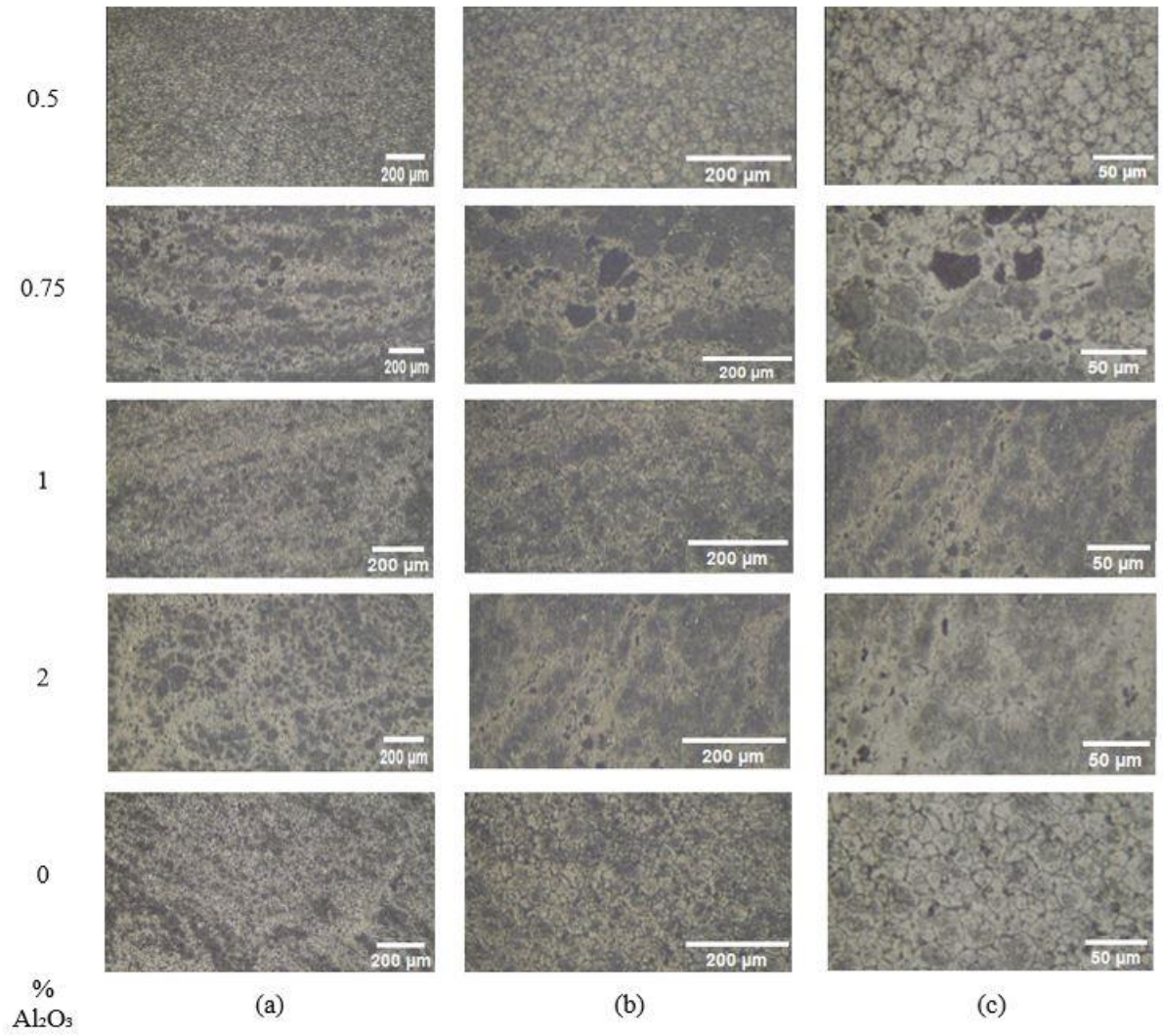


Figure. 22. Metallographic images of the specimens at different magnifications: (a) 100×, (b) 250×, and (c) 400×

Table 3. Comparison of the microstructures of specimens at different reinforcement contents

Al_2O_3 wt.%	Microstructural Characteristics	Particle Distribution
0.5% FSBE AA7020	Medium fine grains, limited agglomerations	Relatively uniform
0.75% FSBE AA7020	Finer than 0.5%, clearer boundaries	More uniform
1% FSBE AA7020	Finest structure, excellent grain growth control	Uniform
20% FSBE AA7020	Fine grains, but more particle agglomerations	Semi-uniform
0% FSBE AA7020	Coarse grains, indistinct boundaries	No reinforcing particles



Figure. 23. Specimens mounted for metallographic examination.

4.4 Hardness Variation Analysis

Specimens with weight percentages of 0, 0.5, 0.75, 1, and 2% aluminum oxide were prepared according to the specified standard for hardness testing. Additionally, hardness tests were also performed on annealed AA7020 and AA7020-T6 specimens to compare them with the other specimens. To investigate the effect of Al_2O_3 reinforcing particle weight percentage on the hardness of AA7020 specimens produced by friction stir back extrusion (FSBE), Brinell hardness testing was conducted on mounted specimens. The test results are presented in Table 4. Hardness measurements were repeated on at least 5 specimens per condition, and the mean values are reported in Table 4. With an increase in the reinforcing particle content, the hardness of the specimens steadily increased. This trend is attributed to the presence of hard Al_2O_3 ceramic particles within the aluminum matrix, which hinder dislocation motion and lead to increased resistance to plastic deformation. Overall, the results indicate that increasing the Al_2O_3 weight percentage leads to a rising trend in hardness, and using these particles as a reinforcing phase in aluminum matrix composites produced by friction stir back extrusion is an effective strategy for improving mechanical properties.

Table 4. Hardness and grain size measurement results for the specimens

Specimen Type	Hardness (HB)	Grain Size (μm)
Annealed AA7020	65±1.6	~50–100
AA7020-T6	123±2.8	~45-90
0% FSBE AA7020	92±2.2	~25–30
0.5% FSBE AA7020	94±2.2	~22–25
0.75% FSBE AA7020	97±2.3	~20–22
1% FSBE AA7020	103±2.5	~20–28
2% FSBE AA7020	105±2.5	~15–18

Figure 24 shows the trend of changes in tensile strength and Brinell hardness of the specimens as a function of Al_2O_3 particle weight percentage. It can also be observed that both properties improve with increasing reinforcement content.

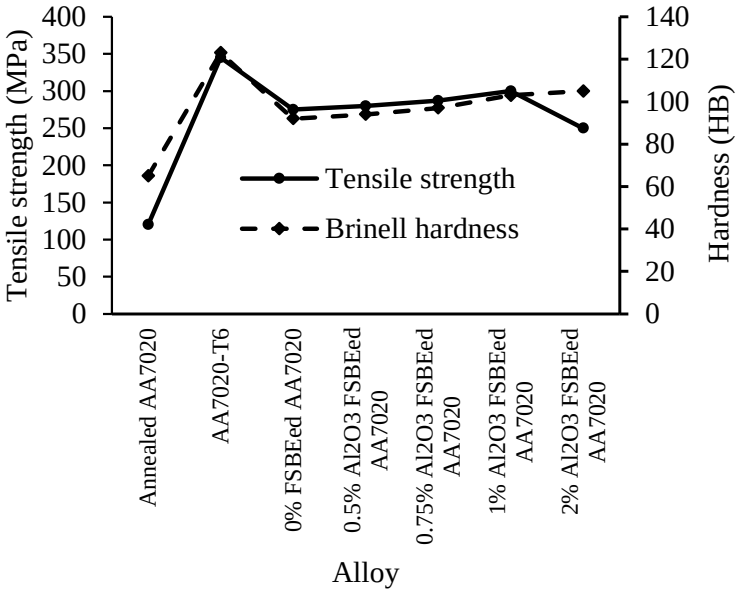


Figure. 24. Comparison of the tensile strength and hardness of specimens produced from different alloys.

4.5 Hardness and Effective Plastic Strain Variations

Due to the nature of the process, variations in hardness and effective plastic strain along the longitudinal direction are negligible and uniform (Figures. 25-27). In contrast, along the radial direction of the specimen, the lowest values of hardness and effective plastic strain are expected at the center, while the highest values occur as the distance from the center increases. The primary factor causing these variations is the frictional shear stress at the peripheral surfaces of the rod. Additionally, torsional shear strains increase with distance from the center, serving as the secondary factor responsible for the changes from the center toward the outer surfaces. Effective plastic strain measured in the longitudinal and radial directions was analyzed in the stabilized region of the rod, after the deformation zone.

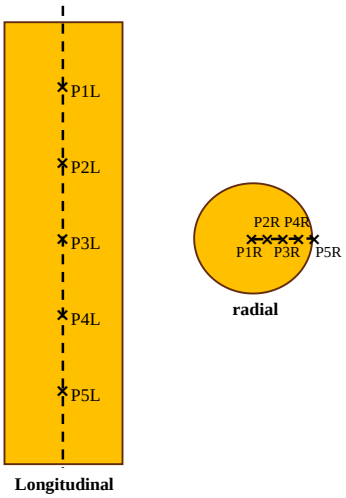


Figure. 25. Locations of hardness measurements and effective plastic strain evaluation along the longitudinal and radial directions.

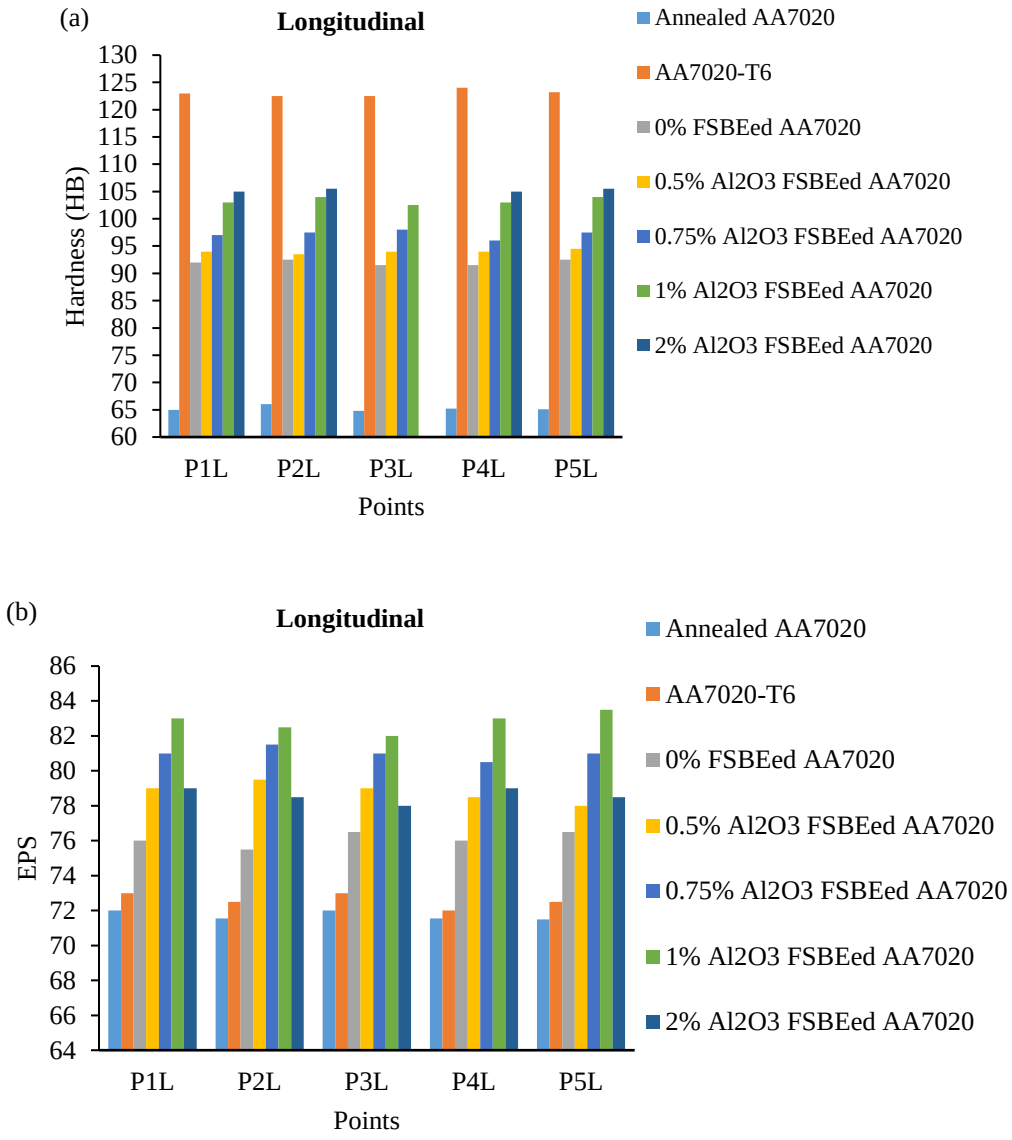
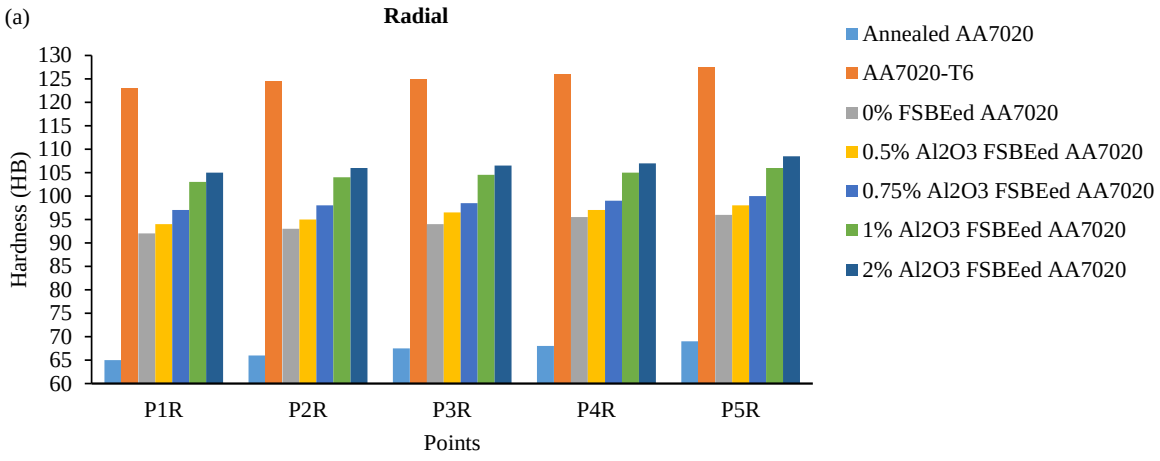


Figure. 26. Variations in (a) hardness and (b) effective plastic strain along the longitudinal direction (uniform distribution).



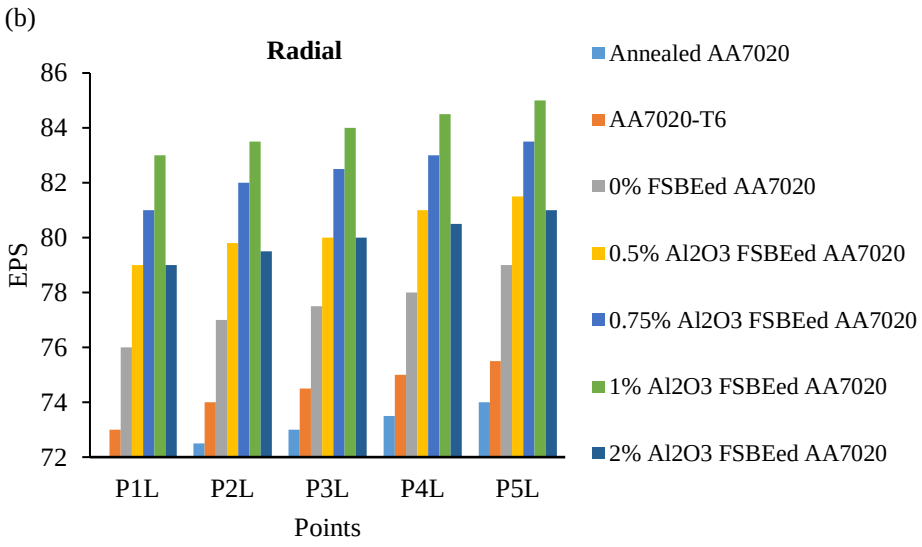


Figure. 27. Variations in (a) hardness and (b) effective plastic strain along the radial direction.

The tensile and hardness test results indicate that the addition of Al_2O_3 particles up to 1 wt.% leads to an enhancement of mechanical behaviors of AA7020 alloys, including an increase in yield and ultimate strength. This improvement can be attributed to factors such as fine-grained structure (due to the role of particles in hindering grain growth), an increase in dislocations (due to the difference in thermal expansion coefficients), and the strengthening of grain boundaries. However, excessive addition of particles (2 wt.%) causes agglomeration of particles and the formation of porosity and other defects, resulting in a reduction in strength and hardness. Moreover, the decrease in elongation of the composite specimens indicates embrittlement of the material, which is related to the presence of crushed oxide networks within the microstructure.

Among the factors that can influence the mechanical properties of the rods produced in this type of process are: the extent of fracture of oxide layers on the chips, the quality of metallurgical bonding between the chips (the higher the quality of this bond, the better the mechanical properties; however, sometimes only mechanical interlocking occurs between the chips and particles, which reduces the quality and mechanical properties), the amount of applied plastic strain (which is significant in this process and has improved the properties of the specimens), the process temperature (between 0.6 and 0.8 of the melting temperature), residual porosity, and subsequent heat treatment (in this study, values were obtained without subsequent heat treatment, such as T6).

5. Conclusion

In this research, the successful production of composite rods from recycled AA7020 chips and Al_2O_3 particles via the FSBE process was demonstrated, and the crucial role of tool design—specifically, the punch with a spiral on its face—in improving material guidance and preventing chip escape was established. The optimal process parameters were determined to be a rotational speed of 450 rpm and a feed rate of 10 mm/min. The results showed that the addition of Al_2O_3 particles up to 1 wt.% improved the tensile properties, with the highest yield strength and ultimate tensile strength reaching

300 MPa and 378 MPa, respectively. However, increasing the particle content to 2 wt.% reduced the yield strength to 250 MPa, the ultimate tensile strength to 300 MPa, and the elongation to 7%. This reduction in tensile performance is primarily associated with particle agglomeration and microstructural inhomogeneity. Although porosity may also contribute to this behavior, its quantitative assessment was not performed in the present study. Nevertheless, the hardness continued to increase with particle content, reaching 105 HB at 2 wt.% Al_2O_3. Finite element simulation showed good agreement with experimental data (temperature of 390–400 °C) and confirmed the influence of punch geometry and contact conditions. Overall, the FSBE method, utilizing the spiral-faced punch, offers a low-energy and sustainable route for the direct recycling of aluminum scrap into composite rods with acceptable mechanical performance without the need for subsequent heat treatment.

Acknowledgements

The authors would like to express their sincere appreciation to all individuals who contributed to and supported this research..

Funding sources

The authors declare that no funds, grants, or other support was received during the preparation of this manuscript.

References

[1] Davis, J. R. (1993). *Aluminum and aluminum alloys*. ASM International.
[2] Association, A. (1984). *Aluminum: Properties and physical metallurgy*. ASM International.
[3] Polmear, I. (2005). *Light alloys: From traditional alloys to nanocrystals*. Elsevier.
[4] Berg, L. K., Gjønnes, J., Hansen, V., Li, X. Z., Knutson-Wedel, M., Waterloo, G., Schryvers, D., & Wallenberg, L. R. (2001). GP-zones in Al–Zn–Mg alloys and their role in artificial aging. *Acta Materialia, 49*(17), 3443–3451. https://doi.org/10.1016/S1359-6454(01)00251-8
[5] Yilmaz, M. S. (2024). Effects of Retrogression and Re-aging (RRA) Processes on Corrosion Properties in AA7020 Aluminium Alloy. *Journal of Materials Engineering and Performance, 33*, 11231–11239. https://doi.org/10.1007/s11665-024-10166-6
[6] Cheng, Q., Ye, L., Huang, Q., Dong, Y., & Liu, S. (2022). Effect of two-stage overaging on microstructure and corrosion properties of an Al-Zn-Mg-Cu alloy. *Journal of Materials Research and Technology, 20*, 1260–1271. https://doi.org/10.1016/j.jmrt.2022.08.098
[7] Mishra, R. S., & Ma, Z. Y. (2005). Friction Stir Welding and Processing. *Materials Science and Engineering: R: Reports, 50*(1-2), 1–78. https://doi.org/10.1016/j.mser.2005.07.001
[8] Gronostajski, J., & Matuszak, A. (2019). Recycling of aluminium alloys by the extrusion of chips. *Journal of Materials Processing Technology, 106*(1-3), 27–32. https://doi.org/10.1016/S0924-0136(00)00530-6
[9] Buffa, G., Campanella, D., Adnan, M., La Commare, U., Ingarao, G., & Fratini, L. (2024). Improving the Industrial Efficiency of Recycling Aluminum Alloy Chips Using Friction Stir Extrusion: Thin Wires Production Process. *International Journal of Precision Engineering and Manufacturing-Green Technology, 11*, 1133–1146. https://doi.org/10.1007/s40684-023-00573-w

[10] Negozio, M., Donati, L., Bocchi, S., & Giardini, C. (2024). Prediction of the microstructure evolution during the friction stir extrusion of a AA6061 aluminum alloy. *Materials Forming, Conference,* 75. doi: 10.21741/9781644903131-75

[11] Bocchi, S., D'Urso, G., & Giardini, C. (2023). Numerical Modeling of a Sustainable Solid-State Recycling of Aluminum Scraps by Means of Friction Stir Extrusion Process. *Materials, 16*(12), 4375. doi: 10.3390/ma16124375

[12] Corre, T., Perrin, J., Gebhard, J., Duchateau, T., Lilensten, L., Laurent-Brocq, M., & Guillou, R. (2024). Tensile and shear behavior of recycled AA 6060 aluminium chips by direct hot extrusion. *Materials Science and Technology, 42*(1):61-67. https://doi.org/10.1177/02670836241287768

[13] Wagiman, A., Mustapa, M. S., Asmawi, R., Shamsudin, S., Lajis, M. A., & Mutoh, Y. (2020). A review on direct hot extrusion technique in recycling of aluminium chips. *The International Journal of Advanced Manufacturing Technology, 106*, 641–653. https://doi.org/10.1007/s00170-019-04629-7

[14] El-Sayed Seleman, M., Ataya, S., Ahmed, M., Hassan, A., Latief, F., Hajlaoui, K., et al. (2022). The Additive Manufacturing of Aluminum Matrix Nano Al2O3 Composites Produced via Friction Stir Deposition Using Different Initial Material Conditions. *Materials, 15*, 2926. doi: 10.3390/ma15082926

[15] Chelladurai, S. J. S., Kumar, S. S., Venugopal, N., Ray, A. P., Manjunath, T. C., & Gnanasekaran, S. (2021). A review on mechanical properties and wear behaviour of aluminium based metal matrix composites. *Materials Today: Proceedings, 37*, 908–916. https://doi.org/10.1016/j.matpr.2020.06.053

[16] Edalati, K., Wang, Q., Enikeev, N. A., Peters, L.-J., Zehetbauer, M. J., & Schafler, E. (2022). Significance of strain rate in severe plastic deformation on steady-state microstructure and strength. *Materials Science and Engineering: A, 859*, 144231. https://doi.org/10.1016/j.msea.2022.144231

[17] Dangwal, S., Edalati, K., Valiev, R. Z., & Langdon, T. G. (2023). Breaks in the Hall–Petch relationship after severe plastic deformation of magnesium, aluminum, copper, and iron. *Crystals, 13*(3), 413. https://doi.org/10.48550/arXiv.2402.11798

[18] Diyoke, G., Rath, L., Chafle, R., Ben Khalifa, N., & Klusemann, B. (2024). Numerical simulation of friction extrusion: process characteristics and material deformation due to friction. *International Journal of Material Forming, 17*(3), 26. doi: 10.1007/s12289-024-01825-z

[19] Hashim, J., Looney, L., & Hashmi, M. S. J. (1999). Metal matrix composites: production by the stir casting method. *Journal of Materials Processing Technology, 92–93*, 1–7. https://doi.org/10.1016/S0924-0136(99)00118-1

[20] Tjong, S. C., & Ma, Z. Y. (2000). Microstructural and mechanical characteristics of in situ metal matrix composites. *Materials Science and Engineering: R: Reports, 29*, 49–113. https://doi.org/10.1016/S0927-796X(00)00024-3

[21] Haddadi, E., Jafarzadeh, H., & Shameli, M. (2025). Numerical and Experimental Study of Backward-Radial Extrusion Process for Flanged Brass Alloy C26000 Parts. *Journal of Materials Engineering and Performance, 35*, 15421-15442. https://doi.org/10.1007/s11665-025-12737-7

[22] Haddadi, E., & Jafarzadeh, H. (2025). Experimental and Numerical Investigation of the Cold Extrusion of a Cup-Shaped Steel Joint Body and the Effect of Die Geometry and Lubrication Parameters. *Amirkabir Journal of Mechanical Engineering, 57*(9), 1107–1126. https://doi.org/10.22060/mej.2026.25074.7919

[23] Ma, Z. (2008). Friction Stir Processing Technology: A Review. *Metallurgical and Materials Transactions A, 39*(3), 642–658. https://doi.org/10.1007/s11661-007-9459-0

[24] Rathee, S., Maheshwari, S., Siddiquee, A. N., & Srivastava, M. (2017). A Review of Recent Progress in Solid State Fabrication of Composites and Functionally Graded Systems Via Friction Stir Processing. *Critical Reviews in Solid State and Materials Sciences, 43*(12), 1–33. https://doi.org/10.1080/10408436.2017.1358146

[25] Abu-Farha, F. (2012). A Preliminary Study on the Feasibility of Friction Stir Back Extrusion. *Scripta Materialia, 66*(9), 615–618. https://doi.org/10.1016/j.scriptamat.2012.01.059

[26] Whalen, S., Olszta, M., Reza-E-Rabby, M., Roosendaal, T., Wang, T., Herling, D., Taysom, B. S., Suffield, S., & Overman, N. (2021). High Speed Manufacturing of Aluminum Alloy 7075 Tubing by Shear Assisted Processing and Extrusion (ShAPE). *Journal of Manufacturing Processes, 71*, 699–710. https://doi.org/10.1016/j.jmapro.2021.10.003

[27] Akbari, M., Asadi, P., Abdi Behnagh, R., Bedir, F., Choupani, N., & Sadowski, T. (2024). Process parameters and tool design in friction stir extrusion: A sustainable recycling technique. *Engineering Reports*, e13006. https://doi.org/10.1002/eng2.13006

[28] Akbari, M., Asadi, P., & Rahimi Asiabaraki, H. (2024). A hybrid method of NSGA-II and TOPSIS to optimize the performance of friction stir extrusion. *Iranian Journal of Materials Forming, 11*(1), 46–62. https://doi.org/10.22099/ijmf.2024.49376.1338

[29] Shahbazi, D., & Asadi, P. (2024). Experimental and numerical investigation of friction stir back extrusion of AA6061 aluminum alloy: Analysis of microstructure, mechanical properties, and temperature distribution. *Proceedings of the Institution of Mechanical Engineers, Part L: Journal of Materials: Design and Applications, 238*(4), 789–805. https://doi.org/10.1177/14644207231204567

[30] Abhilash, V., Lakshmikhanth, R. S., Vignesh, A. R., et al. (2026). Process Optimization and Microstructural Characteristics Correlation in Brass Tube Fabrication by Friction Stir Back Extrusion. *Journal of Materials Engineering and Performance*. https://doi.org/10.1007/s11665-026-13564-0

[31] Mehdipour, M., & Jamshidi Aval, H. (2025). Microstructure Evolution and Corrosion Resistance of As-Extruded AZ91–Ca Alloy During Friction Stir Back Extrusion. *Metallography, Microstructure, and Analysis, 14*, 189–200. https://doi.org/10.1007/s13632-024-01152-4

[32] Mehdipour, M., & Jamshidi Aval, H. (2025). Effect of Plastic Deformation Induced by Friction Stir Back Extrusion on Properties of As-Extruded AZ91-Ca Alloy. *Journal of Materials Engineering and Performance, 34*, 1825–1839. https://doi.org/10.1007/s11665-024-09191-2

[33] El Mehtedi, M., Forcellese, A., Mancia, T., Simoncini, M., & Spigarelli, S. (2019). A New Sustainable Direct Solid State Recycling of AA1090 Aluminum Alloy Chips by Means of Friction Stir Back Extrusion Process. *Procedia CIRP, 79*, 638–643. https://doi.org/10.1016/j.procir.2019.02.062

[34] Hu, M. L., Ji, Z. S., Chen, X. Y., Wang, Q. D., & Ding, W. J. (2012). Solid-State Recycling of AZ91D Magnesium Alloy Chips. *Transactions of Nonferrous Metals Society of China, 22*(1), s68–s73. https://doi.org/10.1016/S1003-6326(12)61685-9

[35] Campbell, J. (2015). *Complete Casting Handbook: Metal Casting Processes, Metallurgy, Techniques and Design*, (2nd Edition). Elsevier. doi: 10.1016/C2014-0-01548-1

[36] Sabau, A. S., & Dinwiddie, R. B. (2008). Characterization of spray lubricants for the high pressure die casting processes. *Journal of Materials Processing Technology, 195*(1-3), 267–274. https://doi.org/10.1016/j.jmatprotec.2007.05.021